

Aerodynamic Performance of Different Trailing-edge Serrations for High Reynolds Number Flows around Wing-flap System

S. Ahmadkhah, A. Jahangirian[†] and A. Zarinvafa

Department of Aerospace Engineering, Amirkabir University of Technology, Tehran, Iran

[†]Corresponding Author Email: ajahan@aut.ac.ir

ABSTRACT

In the present work different trailing-edge serration models are designed and their aerodynamic performances at realistic landing conditions around a wing-flap system are investigated. The serration model with the best performance is then introduced. The NLR 7301 wing and single-slotted flap is selected as reference geometry and three types of serrations in the form of sinusoidal, square, and triangular shapes are cut into the trailing edge of the main element. The flow at Mach number 0.185 and the Reynolds number 2.51 million is calculated by numerical solution of incompressible Navier-Stokes equations using $k-\epsilon$ realizable turbulence model. Results show that the serration has exceptional positive effects on the aerodynamic characteristics of the system by generating vortices that modify the flow structure downstream of the main airfoil. All serrated models experience a reduction in drag coefficient compared to the baseline model at incidence angles before stall. Additionally, the maximum lift coefficients for all serrated models are increased. Among the serrated models, the sinusoidal serration exhibits the best performance with 6.8% increase in the maximum lift coefficient, a 10.6% decrease in the drag coefficient, and 2 degrees increase in the stall angle of attack of the wing-flap system compared to the baseline geometry. Moreover, the effect of wavelength on the performance of square shape serration is investigated and its aerodynamic advantages and disadvantages are presented.

Article History

Received June 22, 2024

Revised November 28, 2024

Accepted December 1, 2024

Available online February 4, 2025

Keywords:

Wing-flap system

Trailing edge serration

Aerodynamic performance

High Reynolds number flow

Turbulent flow

1. INTRODUCTION

Flaps play a vital role in increasing the performance and safety of the aircraft, especially in low-speed situations like landing and take-off (Jahangirian & Johnston, 2007). These moving surfaces, which are usually located on the trailing edge of aircraft wings, by increasing the lift force, enable the plane to take off and land at lower speeds. Slotted flaps consist of several small individual airfoils. The gap between the flap and the wing helps the movement of high-pressure air moving from under the wing to the upper surface re-energizing the boundary layer, that may cause delaying flow separation from the flap (Young, 1947).

In the past years, some studies have implemented passive and active flow control systems, while others studied on the feasibility of completely new systems, such as morphing wings and Plasma actuators (Khoshkhoo & Jahangirian, 2016; Nemati & Jahangirian, 2020). However, these methods are often really complex and require actuation systems, compressed air and extensive

power to operate. Another conventional passive control system is the use of vane vortex generator. These devices can be installed on the wing or the flap of high-lift devices to suppress flow separation (Ichikawa et al., 2021). However, in normal conditions these devices perform no useful function and exert a significant drag penalty (Saddoughi, 1994).

The use of serration on the trailing edge of a single wing element have also been investigated. In 1970s, Hersh et al.'s experiments on acoustic resonance showed that the use of serrations on aerodynamic surfaces can reduce the aerodynamic noise of the flow (Hersh & Hayden, 1971). But the flow mechanism causing this remained unclear. Gruber et al. compared the trailing edge noise reduction using saw-tooth and slit serrations on a NACA651210 airfoil. However, these are shown to be considerably less than theoretical predictions (Gruber et al., 2010). Also, they suggested that the flow mechanisms by which serrated trailing edges reduce noise are not yet fully understood. Singh et al. (2022) investigated the efficacy of sinusoidal trailing-edge serrations for noise

NOMENCLATURE			
C_D	drag coefficient	v	velocity
C_p	pressure coefficient	Y^+	surface non-dimensional normal distance
C_L	lift coefficient	α	angle of attack
h	amplitude	λ	wave length
p	static pressure	ν	kinematic viscosity
Re	Reynolds number	ρ	density
t	time		

reduction purposes. Results showed that trailing-edge serrations reduce leading-edge noise along with the self-noise, which indicates the efficacy of trailing-edge serrations in reducing the far-field noise. [Tlua and Joana \(2020\)](#) investigated the reduction of Turbulent Boundary Layer Trailing Edge (TBL-TE) interaction noise on NACA 0012 airfoil and flat plate. Results showed that serrated trailing edge configurations can yield less TBL-TE noise compared to the baseline. In a study by [Wei et al. \(2024\)](#) a bioinspired propeller design featuring novel three-dimensional sinusoidal serrations on the propeller's topology demonstrated improvements in both noise reduction and aerodynamic efficiency. Experimental results revealed a reduction in overall sound pressure levels by up to 5.5 dB and an increase in propulsive efficiency of more than 20%. [Jawahar et al. \(2020\)](#) performed experimental measurements to assess the aero-acoustic properties of 30P30N airfoil with two different types of serrated slat cusps. The far-field noise measurement results showed that significant noise reduction at the vortex shedding frequency can be achieved by the use of serration and No-Cusp configuration. [Alawadhi et al. \(2014\)](#) studied the wing and flap with a triangular serration on the trailing edge of the main wing with variable serration angle relative to the wing chord. They showed that larger deflection induces stronger vortices. Also, serration energizes the boundary layer and encourages the flow to remain attached to the flap. [Hussain et al. \(2017\)](#) performed computational and experimental study on NACA0012 wing section with serrated trailing edge. Two types of triangular and quadratic serrations, were investigated for their influence primarily on lift to drag ratio of the wing. Serrations tend to enhance both aerodynamic and aero-acoustic parameters and there is direct increase in the coefficient of lift, caused by introducing trailing edge serrations. [Ethiraj and Pillai \(2021\)](#) investigated the aerodynamic characteristics of NACA series airfoils by altering the trailing edge in the form of extended and serrated sections. NACA 0020 airfoil was experimentally studied at the angle of attack ranging from 0° to 45° and for the Reynolds number of 2.46×10^5 . All serrated trailing edge delay stalling compared to the baseline model. Serrated edge modification favors smooth stall and thereby acts as an effective flow control device. [Chandra and Sharma, \(2017\)](#) carried out experimental investigation on a low aspect ratio wing at the Reynolds number of 7.6×10^4 with sinusoidal serration at various wavelengths. It was observed that applying the sinusoidal serrations at the leading edge reduces the aerodynamic efficiency of the wing. However, when the serrations are placed at the trailing edge the aerodynamic efficiency in terms of CL/CD improves compared to the clean wing. [Naeini et](#)

[al. \(2019\)](#) studied the effect of nature-inspired leading edge 3D serration on the aerodynamic performance of a 65/35-degree double delta wing in a low-speed wind tunnel. It was concluded that compared to the clean model, there is a notable enhancement in the maximum lift coefficient. A drag reduction is also achieved by installing these elements, which provided a higher lift-to-drag ratio for all incidence angles. Finally, the serrated leading edge postponed the stall angle of the double delta wing. [Knepper and Garry \(2005\)](#) carried out experimental studies on a wing and single-slotted flap with triangular serrations on the trailing edge and showed that a serrated trailing edge can enhance slotted flap performance at specific flap lap/gap settings and flap deflections ([Knepper & Garry, 2005](#)). The results confirm that longitudinal vortices in the wake of the serrations, delay flow separation on the upper surface of the flap. [Catalano et al. \(2007\)](#) carried out experimental and numerical studies on a wing-flap model with only triangular serrations at Reynolds number around. Results showed that vortices are formed at the saw-toothed trailing edge through the mixing between the flow from the pressure side to the suction side at the main wing and flap gap. Serrated trailing edge can therefore, improve the flow over the flap by delaying flow separation consequently decreasing pressure drag. [Liu et al. \(2019\)](#) performed experimental study on the application of trailing-edge serrations as a passive control method for reducing the unsteady aerodynamics loading and noise on airfoils in tandem configurations. Flow experiments were performed using saw-tooth serration with different wavelength, for several tandem airfoil configurations. Another study on the NACA0012 airfoil showed that the serrations have significant aerodynamic effects ([Ji et al., 2023](#)).

As mentioned before, enhancing the efficiency of high-lift devices is crucial for improving flight safety and passenger comfort, both of which are of utmost importance in the aviation industry. Previous studies indicated that the serrations can increase the energy of the flow downwind. Moreover, increasing boundary layer energy can result in higher lift coefficients. Despite existing research, the aerodynamic effects of trailing edge serrations in wing-flap systems, particularly at realistic Reynolds and Mach numbers, as well as the influence of serration patterns on system performance, remain unexplored. Thus, in the present study the turbulent flow around wing-flap systems with several trailing edge serrated models at high Reynolds number flow conditions are investigated. The effects of the serration type (square, sinusoidal and triangular) and the wavelength of the serration on the aerodynamic performance of the system are discussed. Additionally, insights into the underlying

Table 1 Properties of the 2D grids

	Coarse	Medium	Fine	Very Fine
Number of Elements	15141	31553	47184	80016
Inflation Layer	6	8	11	13
Growth rate	1.29	1.22	1.2	1.2
Element size (on airfoil)	0.012	0.0075	0.005	0.003
C_l	2.36363	2.36945	2.37436	2.37424
Error% (Narsipur et al., 2012)	1.29	1.05	0.84	0.85

flow structure, lift generation, and drag reduction of the system have also been presented.

2. NUMERICAL FLOW SOLUTION METHOD

2.1 Governing Flow Equations

In this study, the governing equations of the flow are the conservation of mass, and momentum. The conservation of mass (continuity) equation in the differential form is presented in Equation (1) where ρ is density and \vec{v} is the velocity vector (Batchelor, 2000):

$$\nabla \cdot (\rho \vec{v}) = 0 \quad (1)$$

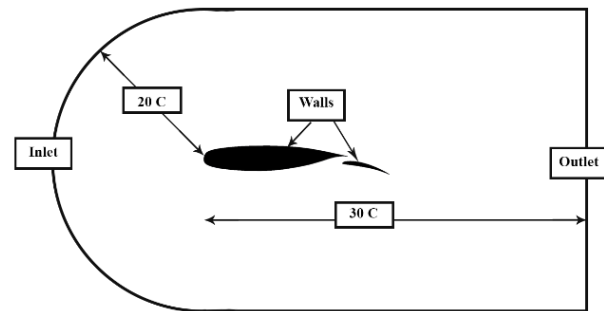
The linear momentum conservation equation is obtained from Newton's second law of motion that can be shown in Equation (2) (Batchelor, 2000):

$$\frac{\partial}{\partial t} (\vec{v}) + (\vec{v} \cdot \nabla) \vec{v} = -\frac{1}{\rho} \nabla P + \nu \nabla^2 \vec{v} \quad (2)$$

In this equation, P is the static pressure and ν is kinematic viscosity. Due to low subsonic speed of the flow in this study, it can be considered incompressible. As a result, there is no need for the energy equation and it is possible to simulate the flow acceptably with the conservation of mass and momentum. After examining different turbulence models and comparing their accuracy and computational cost, it was decided to use the $k-\epsilon$ Realizable turbulence model with wall function settings near the walls. This model, while being relatively simple, has acceptable results. Furthermore, the model allows using bigger cells near the wall up to $y^+ = 20$. Therefore, the number of elements is reduced and the computational cost especially in the 3D problems are decreased significantly.

2.2 2D Grid Study

After examining different wing and flap models to implement the idea, the reference geometry NLR 7301 wing-flap model is selected which has a complete set of experimental databases (Van den Berg & Gooden, 1994). This configuration is designed that no flow separation occurs on the main element, apart from a small laminar separation bubble on the wing nose. The 32% chord flap is deflected 20 degrees. The experiments for this wing have been carried out at Reynolds number 2.51 million and Mach number of $M = 0.185$ (Van Den Berg & Gooden, 1994). For grid study and to validate the solver, a 2D flow around the reference geometry is selected from which the experimental data are available. Considering the complexity of the geometry and the requirements of the

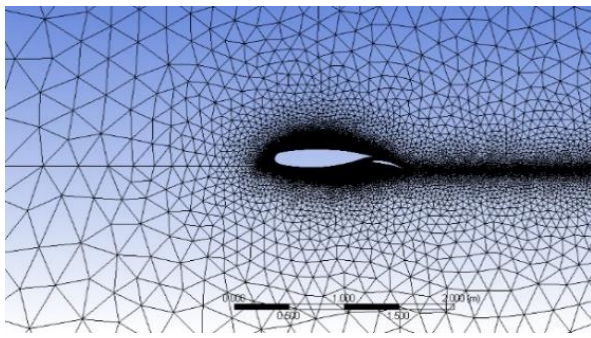
**Fig. 1 2D domain and boundary conditions**

problem, a hybrid grid is used, in such a way that the boundary layer is discretized by a structured grid and the rest of the domain is unstructured. Also, a C-type domain with an inlet radius 20 times the chord length and an outlet distance 30 times the chord length was used (Fig. 1).

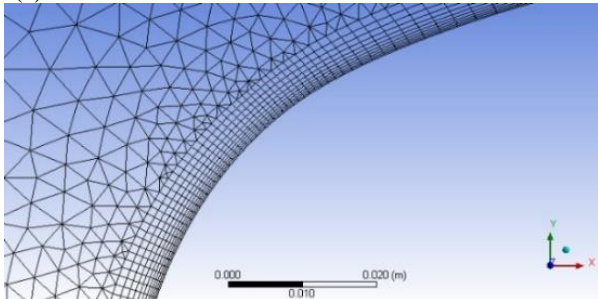
To ensure that the results are grid-independent, different 2D grids were generated (namely coarse, medium, fine and very fine grids) and the results are presented in Table 1. Considering the lift coefficient values the fine grid is chosen as the proper grid for the numerical solution (Fig. 2).

2.3 Flow Solution Method

All the solutions are steady state and the effect of gravity is ignored. A pressure-velocity coupling approach is utilized and the equations are discretized with a second-order accurate upwind method. Also, the Courant number is set at 200. To verify the results, it is necessary to compare them with experimental data. For this purpose, the experimental data from AGARD (Van Den Berg & Gooden, 1994) is used. The flow conditions are Mach 0.185 and the Reynolds number of 2.51 million. Also, considering the grid study results, the Fine grid with 47184 elements is used for the validation computations. In Fig. 3, the surface pressure coefficients from the experimental data and the numerical results for the angles of attack 6 and 13.1 degrees are presented. Due to this figure, it can be concluded that the validation was successful. All numerical computations were done on a computer system equipped with an Intel(R) Core (TM) i7-4790K processor with a frequency of 4.00 GHz and 32 GB RAM. As a reference, the sinusoidal model at 6 degrees AOA took about 6 hours to complete 500 iterations and reach converged solution in this system.

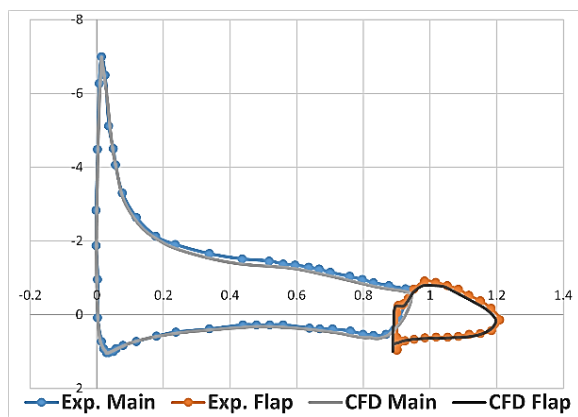


(a) full view

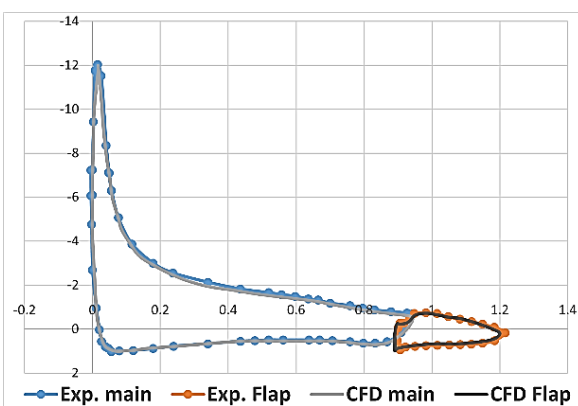


(b) Zoomed in

Fig. 2 Fine Grid



(a) AOA=6°



(b) AOA=13.1°

Fig. 3 Surface Pressure Coefficients at Re=2.51E6 and Mach=0.185 (Van Den Berg & Gooden, 1994)

2.4 Design of Serrations

With the studies conducted on different serration patterns, three patterns of sinusoidal, square, and

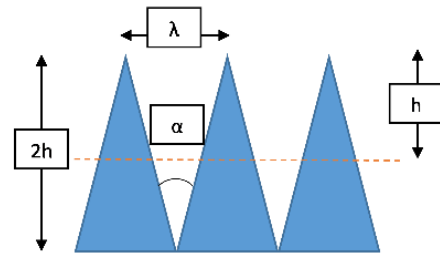


Fig. 4 Serration Geometry

Table 2. Serration pattern properties

λ/h	$2h$	λ
1.5	47mm	35.25mm
0.6	47mm	14.1mm

triangular with wavelength to amplitude ratio of 1.5 ($\lambda/h = 1.5$) on the trailing edge of the main wing are applied. Also, to compare and investigate the effect of the ratio of wavelength to amplitude, a square wave model with a ratio of 0.6 ($\lambda/h = 0.6$) has been studied. The chord length of the main airfoil of the base model is equal to 940 mm. According Fig. 4 the length of the tip to the bottom of the serrations are set to be 5% of the chord length which is equal to 47 mm. This amount is twice the wave amplitude (Table 2). To be able to only examine the effect of the serrations, patterns were cut into the main wing element as shown in Fig. 5.

To better investigate the effect of serrations on the performance of the system, with a minimum number of grid elements, the 3D model is used with symmetry boundary conditions. Using symmetry boundary conditions allow to only study the serration effects and a shorter span is numerically calculated. Hence, the computational cost is decreased. To consider the effect of serrations on each other, three serrations are used next to each other. But in the square wave pattern with the ratio 0.6 ($\lambda/h = 0.6$), it was decided to use nine serrations instead of three so that the model has a similar span to the other serrated models.

2.5. 3D Boundary Conditions and Validation

According to the simulation conditions, the inlet boundary condition is “Velocity Inlet” and the outlet boundary condition is “Pressure Outlet”. Also, all the walls on the wing’s surfaces have the wall boundary condition. Boundary conditions and the domain size are displayed in Fig. 6. Also, the inlet pressure is equal to 101325 Pa.

To generate a proper 3D mesh, the settings of the 2D fine grid specified in section 2-2 including the sizes on the wing, the boundary layer sizes, etc., are used as a reference. For a more accurate simulation, the sizes of the cells on the serrations is slightly smaller, therefore, the number of cells of the grids produced for the baseline, triangular, sinusoidal, square ($\lambda/h = 1.5$), and square ($\lambda/h = 0.6$) models are respectively 2.1, 2.2, 2.6, 2.1 and 3.1 million. The generated 3D grids are shown in Fig. 7. The

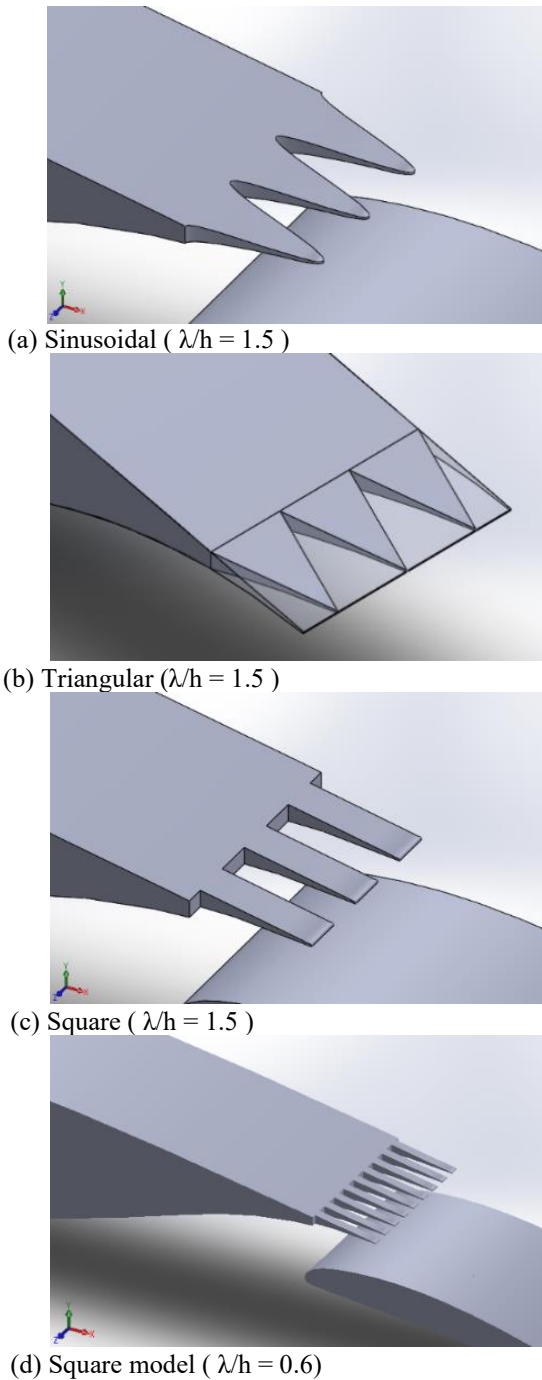


Fig. 5 NLR 7301 wing and flap with serrated trailing edge

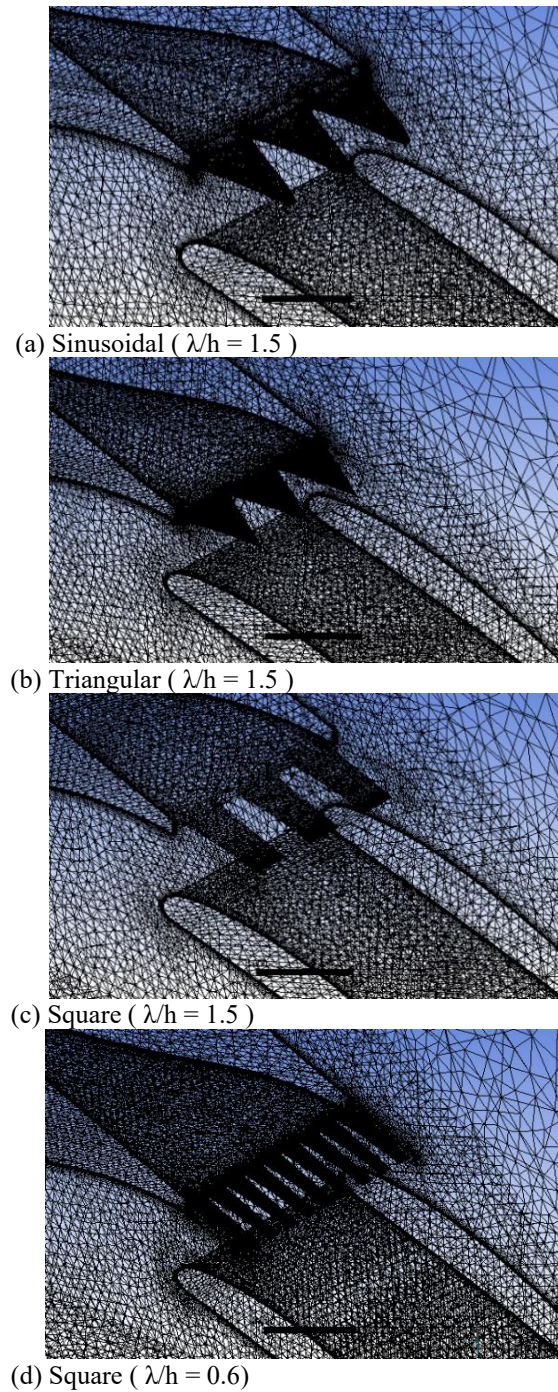


Fig. 7 3D Grids for the serrated models

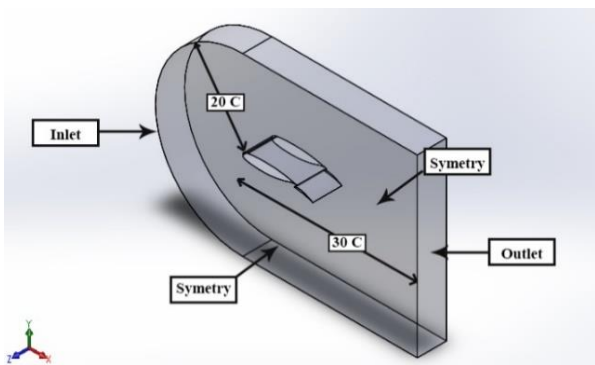
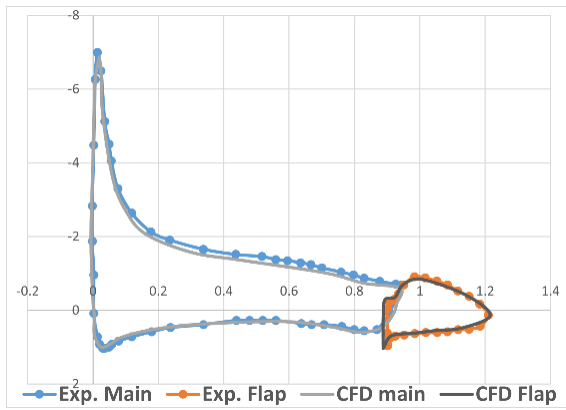
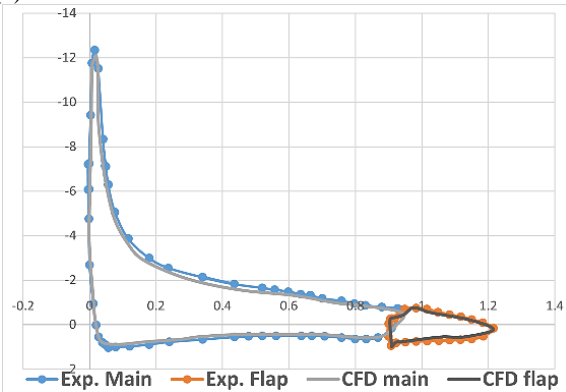


Fig. 6 3D Domain and Boundary Conditions

skewness and orthogonality are used as the primary criterion for preliminary grid evaluation. In this case, the average skewness values for generated grids around serrated cases are between the ranges of 0.269-0.399, which are within the acceptable range. The average orthogonality values are also between the range of 0.688 and 0.699 which are again within the acceptable range. Nevertheless, among about 3 million 3d grid cells, there may be some cells with low quality measures. For example there are a few number of cells with maximum skewness up to 0.999 and/or minimum orthogonality values around 1e-3. However, these extreme values occur for grid cells near the outer boundary where no important features are present that can affect the results. It is noted that the above discrepancy is mainly due to the fact that the span size of



(a) AOA=6°



(b) AOA=13.1°

Fig. 8 3D Surface Pressure Coefficients at Re=2.51E6 and Mach=0.185 (Van Den Berg & Gooden, 1994)

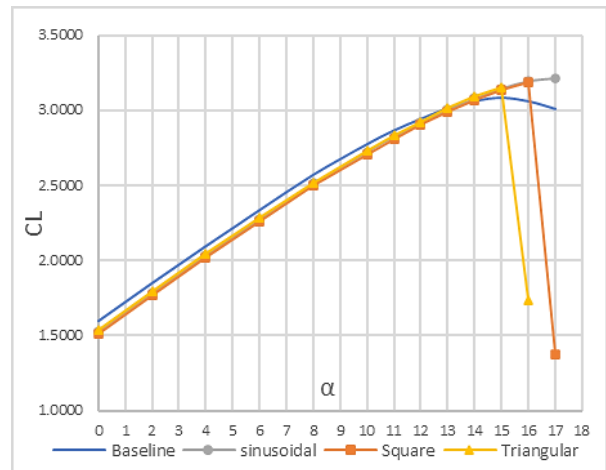
the domain is very smaller than other two domain sizes (see Fig. 6).

The surface pressure distributions obtained from the current numerical method computed at the middle of the wing span baseline model (without serrations) is compared to the experimental data at the angles of attack 6 and 13.1 degrees in Fig. 8. The results are with good agreement that confirms the validity of the method for 3D calculations.

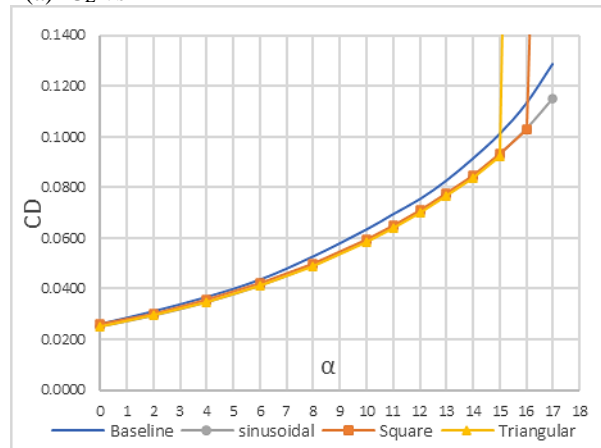
3. RESULTS

In this section, the numerical results of four serrated models that were introduced in the previous section are presented and compared to those of the baseline model (without serration). The simulations are performed at Mach number 0.185 and the Reynolds number of 2.51 million which are similar to the experiment conditions in AGARD (Van Den Berg & Gooden, 1994). The effects of the serrated wing-flap system on the aerodynamic coefficients, including lift, drag and aerodynamic performance (L/D) are analyzed in the following.

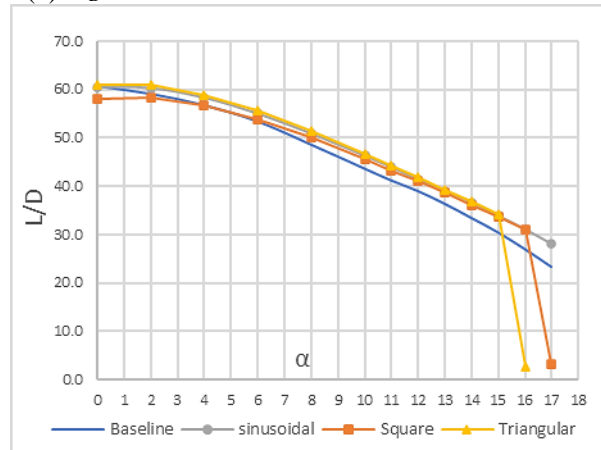
According to Fig. 9a, it can be generally seen that all serrated models except the triangular one have higher maximum lift coefficients and stall angles compared to the baseline model. This is very important since flaps are generally used in landing and take-off conditions in which the angle of attack is usually high. This figure also shows that the gradual stall behavior of the base model has changed to the sudden stall in the triangular and square



(a) C_L vs α



(b) C_D vs α



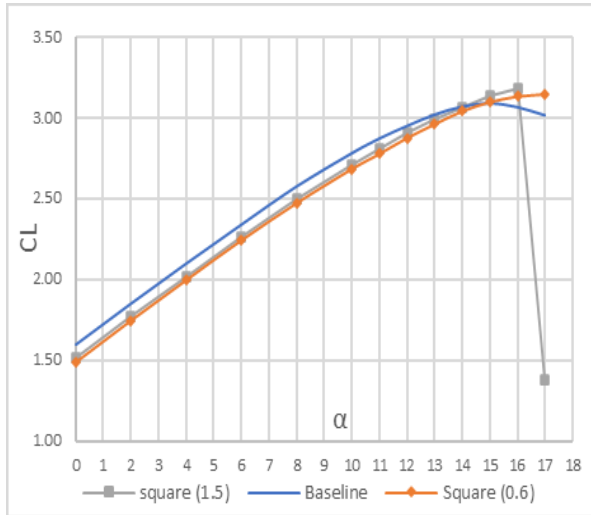
(c) L/D vs α

Fig. 9 Aerodynamics coefficients diagrams for $\lambda/h = 1.5$ models at Re=2.51E6 and Mach=0.185

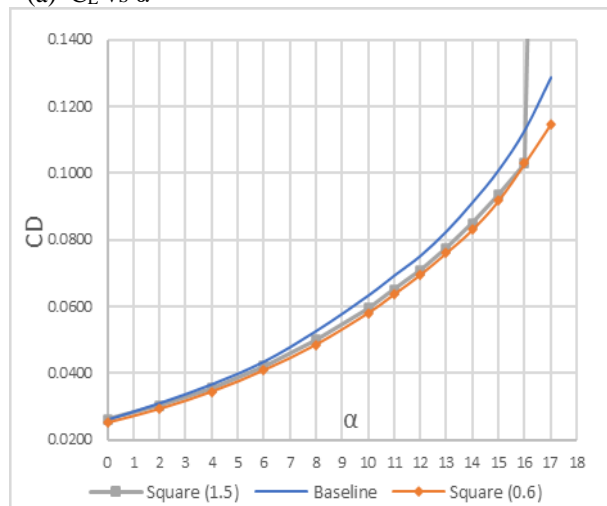
models. This is mainly due to the leakage of the flow from lower surface of the main element through serrations to the upper surface that accelerates the flow separation from the main element upper surface. Among different serration models, the sinusoidal model has higher maximum lift coefficient compared to other models which is 6.8 percent greater than the baseline model. Figure 9b shows that the drag coefficients of the serrated models are less than the baseline model in all incidence angles before stall which is due to separation control above the flap by flow vortices initiated from serrations. In the best case, the sinusoidal

Table 3 Break down of different models Lift Coefficients at AOA=6°

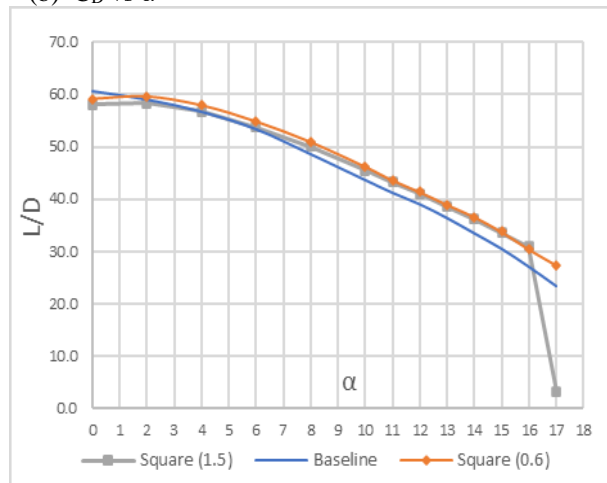
Serration Type	Flap	Wing	Total	Wing's increment (%)	Flap's increment (%)
Baseline	0.331	2.005	2.336	-	-
Triangular	0.374	1.912	2.286	-4.7	13.0
Sinusoidal	0.377	1.900	2.277	-5.2	13.8
Square ($\lambda/h = 0.6$)	0.382	1.857	2.240	-7.4	15.5
Square ($\lambda/h = 1.5$)	0.383	1.877	2.261	-6.4	15.9



(a) C_L vs α



(b) C_D vs α



(c) L/D vs α

Fig. 10 Aerodynamics coefficients diagrams for $\lambda/h = 1.5$ models at $Re=2.51E6$ and $Mach=0.185$

model has a 10.6% reduction in the drag coefficient at an attack angle of 17 degrees compared to the baseline model. Figure 9c demonstrates that the aerodynamic efficiency factors of the serrated models are improved for almost all models in the full range of incidence angles compared with the base model. It can be seen that as the angle of attack increases, the aerodynamic performance of the system also increases and at the incidence angle of 17 degrees, the aerodynamic performance coefficient (L/D) of the sinusoidal model showed a significant increase of 19.53% compared to the baseline model (without serration). It should be noted that this improvement is achieved despite that the serrations are cut into the wing, and the area of the wing is reduced compared to the baseline model.

Figure 10 shows the effect of λ/h ratio on the aerodynamic coefficients at different incidence angles. As demonstrated in this figure the square serrated model with the ($\lambda/h = 0.6$) has better performance than ($\lambda/h = 1.5$) particularly at the stall conditions.

In order to analyze the contributions of the wing and flap in the lift coefficients value at different incidence angles of 6, 15, 16 and 17 degrees, Tables 3, 4, 5 and 6 are presented. It can be seen that in all incidence angles the presence of serrations increases the flap lift coefficient, especially in the higher angles of attack close to the stall. As indicated in Table 3, at the low incidence angle of 6 degrees, the serrated models exhibit 2%-4% less total lift coefficient in comparison with the base line model. However, the flap lift coefficients are increased in all serrated sections with the square model ($\lambda/h = 1.5$) showing the best performance by 15.9% increase compared to the baseline model. It should be noted that the main wing's lift coefficient in all models is slightly decreased in this angle of attack, which can be partly attributed to the reduction of the wing's area.

Tables 4, 5 and 6 are provided for results at higher angles of attack close to the stall. It can be observed that at these incidence angles unlike the 6 degree results, the lift coefficients of the complete system with the serration have been increased. It is notable that the lift coefficient of the main wing has also been increased in some cases. In these ranges of incidences, the sinusoidal type serration shows the best performance with the highest C_{Lmax} and α_{stall} and positive impact on the lift coefficient of both wing and flap. Independent examination of wing and flap coefficients for different wavelengths shows that the square model with ($\lambda/h = 0.6$) has more stable performance than ($\lambda/h = 1.5$) model particularly at the 17° incidence angle.

In Fig. 11, the velocity contours of the sinusoidal model and the baseline at 17 degrees angle of attack are

Table 4 Break down of different models Lift Coefficients at AOA=15°

Serration Type	Flap	Wing	Total	Wing's increment (%)	Flap's increment (%)
Baseline	0.290	2.795	3.085	-	-
Triangular	0.344	2.806	3.151	0.4	18.7
Sinusoidal	0.348	2.797	3.146	0.1	20.0
Square ($\lambda/h = 0.6$)	0.351	2.745	3.096	-1.8	21.2
Square ($\lambda/h = 1.5$)	0.355	2.774	3.130	-0.7	22.4

Table 5 Lift Coefficients break down of different models at AOA=16°

Serration Type	Flap	Wing	Total	Wing's increment (%)	Flap's increment (%)
Baseline	0.280	2.782	3.062	-	-
Triangular (Separation)	0.615	1.120	1.735	-59.7	119.7
Sinusoidal	0.342	2.855	3.197	2.6	22.2
Square ($\lambda/h = 0.6$)	0.344	2.786	3.131	0.2	23.0
Square ($\lambda/h = 1.5$)	0.349	2.835	3.184	1.9	24.7

Table 6 Break down of different models Lift Coefficients at AOA=17°

Serration Type	Flap	Wing	Total	Wing's increment (%)	Flap's increment (%)
Baseline	0.278	2.735	3.013	-	-
Triangular	Complete Separation				
Sinusoidal	0.337	2.880	3.217	5.3	21.4
Square ($\lambda/h = 0.6$)	0.339	2.807	3.146	2.6	22.1
Square ($\lambda/h = 1.5$) (Separation)	0.336	0.985	1.321	-56.2	-64.0

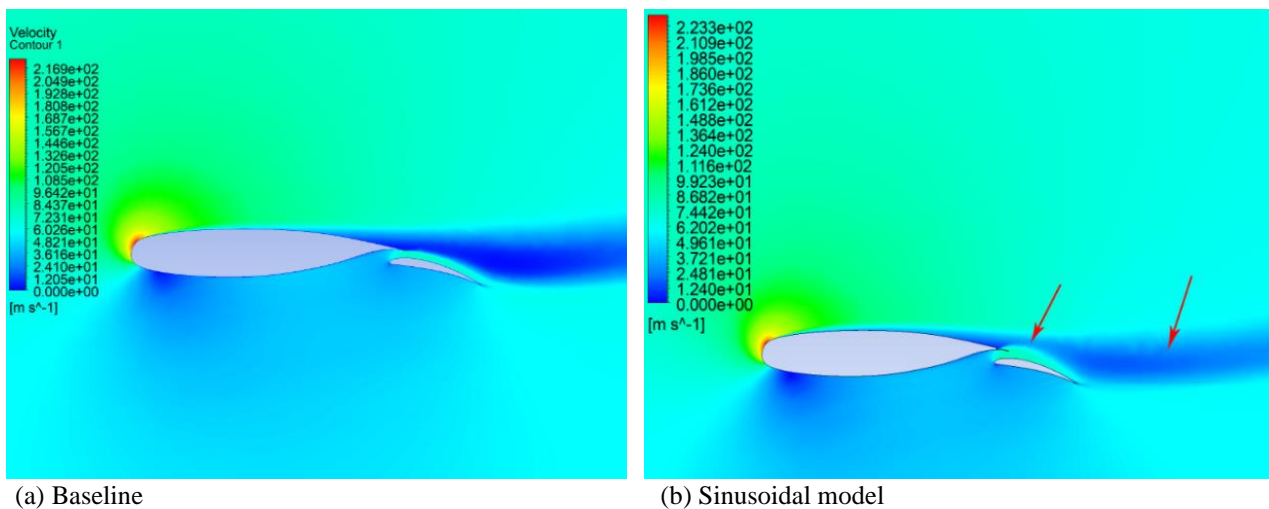
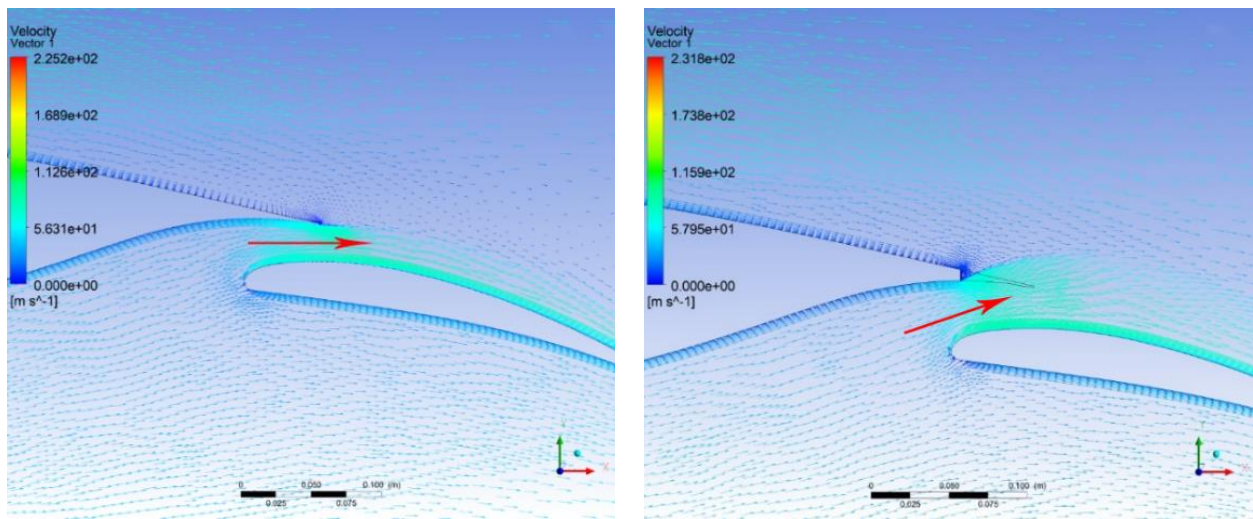


Fig. 11 Velocity contours at AOA of 17 degrees, $Re=2.51E6$, and $Mach=0.185$

presented. It can be seen from this figure that the serrations have several important effects on the flow. First, the shear layer (vortex line) behind the main element, which is strongly present in the baseline model, is considerably weakened in the serrated model. The second important effect is the growth of the high-speed flow layer on the upper surface of the flap which can be one reasons for increasing the flap's lift coefficient. Figure 12 shows the velocity vectors around the wing-flap geometry of the base model and the sinusoidal model at 17° incidence angle. As demonstrated, in the serrated model the flow accelerated between the wing and the flap passes through the teeth at a high-speed generating a vortex flow above the flap. By comparing Figs. 11 and 12, it can be inferred that the serrations enhance the boundary layer energy, allowing

the flap to bear a higher aerodynamic load. Additionally, the weakened shear layer is likely the primary factor contributing to the drag reduction observed in the serrated models.

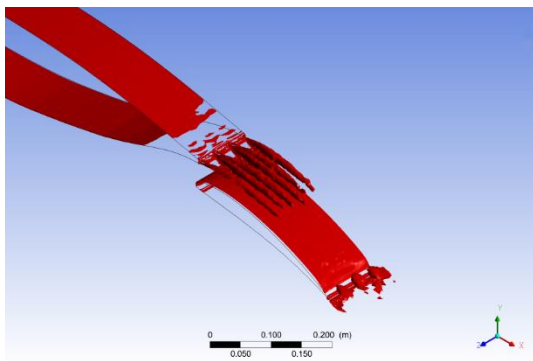
According to the data obtained from the simulations, it can be seen that the serrations generate vortices behind the trailing edge of the main element. Also, studies show that the serration patterns have an important effect on the shape and size of these vortices. The Q-criterion surfaces with the level of 0.002 for all models at an angle of attack 16 degrees are presented in Fig. 13. It should be noted that the triangular serration model is experiencing separation at this angle of attack. In fact, by comparing the Q-criterion surfaces in three areas i.e. close to the trailing edge of the main element upper surface, the wake behind



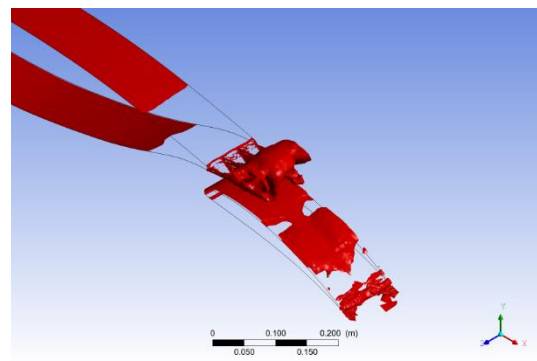
(a) Baseline

(b) Sinusoidal

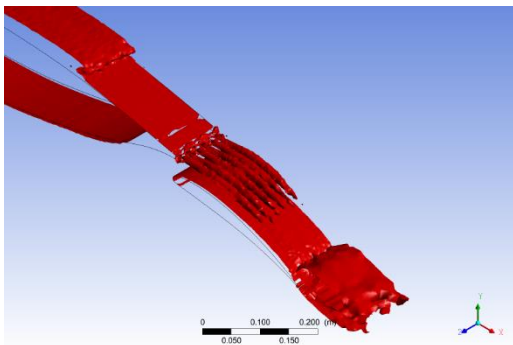
Fig. 12 Velocity Vectors at AOA=17°, Re=2.51E6, and Mach=0.185



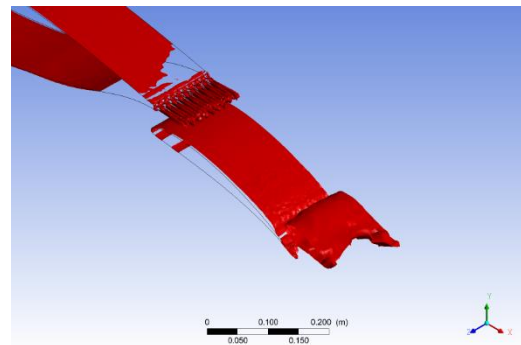
(a) Sinusoidal model



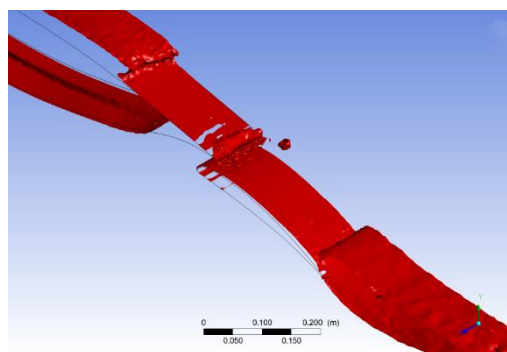
(b) Triangular model (Separation)



(c) Square model ($\lambda/h = 1.5$)



(d) Square model ($\lambda/h = 0.6$)



(e) Baseline model

Fig. 13 Q-Criterion surfaces (0.002) for all models at the AOA of 16 degrees, Re=2.51E6, and Mach=0.185

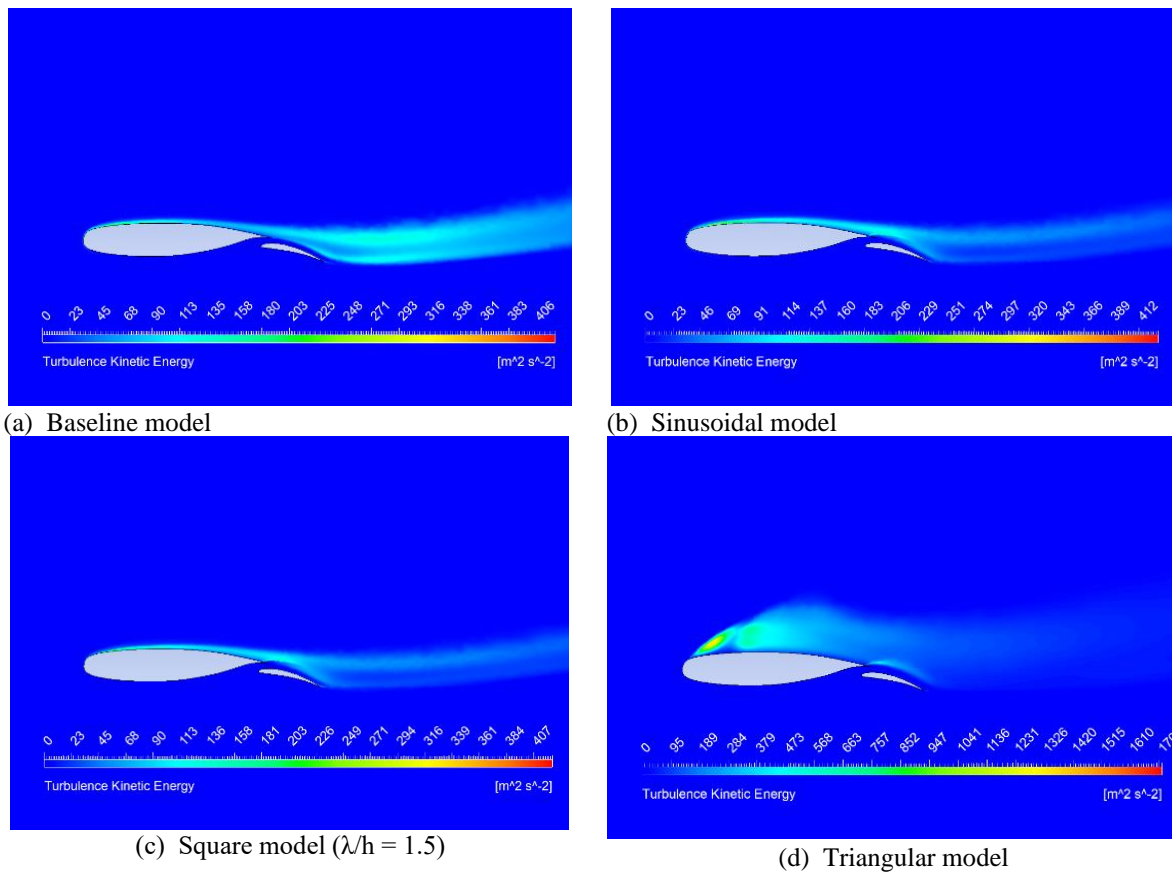


Fig. 14 Turbulent kinetic energy contours for $\lambda/h = 1.5$ models at $AOA = 16^\circ$, $Re=2.51E6$ and $M=0.185$

the trailing edge of the main element, and flap upper surface, one can analyze the influence of different serration models on the flow. It can be seen that the flow passes through the serrations, mixes and produces turbulent vortices above the flap that increase the energy of the flow and delay separation on the flap upper surface. However, this mechanism may also affect the stability of the upstream flow that in the case of triangular serration, produces early flow separation on the main airfoil. The above conclusion can also be confirmed from Table 5 where the contributions of the wing and flap on lift production is presented. Therefore, it can be concluded that the existence of serrations can delay the separation on the flap. In addition, this figure shows that the sinusoidal model has the more stable flow above the wing and flap.

Figure 14 shows the contours of the turbulent kinetic energy at 16-degree angle of attack. According to this figure that displays the turbulent eddies, the triangular model (Fig. 14d) is experiencing a leading edge separation. Based on Fig. 9a, the Baseline model is stalling at the incidence angle of 16 degrees. However, this is a gradual stall from trailing edge of the main element which is different to those of the triangular serrated model. It is evident that in this angle of attack the sinusoidal and rectangular serrations perform better than triangular serration and baseline model. Figure 15 demonstrates the turbulent kinetic energy contours at 17 degree angle of attack which is the post stall condition of the wing flap system. At this angle, the flow over triangular model is not displayed since it was already separated from the leading edge. As it is shown, in this condition the square serrated

model has separated from the leading edge while the flow around the wing with sinusoidal serration has attached yet.

As shown in Fig. 9a, the serrated models demonstrate lower drag coefficients than the baseline models. Therefore, it is reasonable to conclude that the reduction in drag coefficient is directly related to the decrease in turbulent kinetic energy behind the system, resulting from the presence of serrations.

To better investigate the mechanism of lift generation, and the differences between the serrated models and the baseline model, the surface pressure coefficients of the baseline and the sinusoidal model at 17 degrees angle of attack is presented in Fig. 16. It is noted that the pressure coefficient diagram is derived from the middle of the span. According to this figure, the main wing's surface pressure coefficients of the baseline model and the sinusoidal model are almost identical, except for the end part where the serrations are cut into the wing in the sinusoidal model. However, the surface pressures along the flap leading edge area are so different that may cause much higher lift coefficient in the serrated model. According to Fig. 16, this difference is largest at the front of the flap, and when moving toward the end of the flap, the diagrams coincide.

4. CONCLUSIONS

This study examined the impact of different trailing-edge serration patterns on the aerodynamic performance of the NLR7301 wing-flap configuration at high Reynolds number conditions. Numerical simulations were

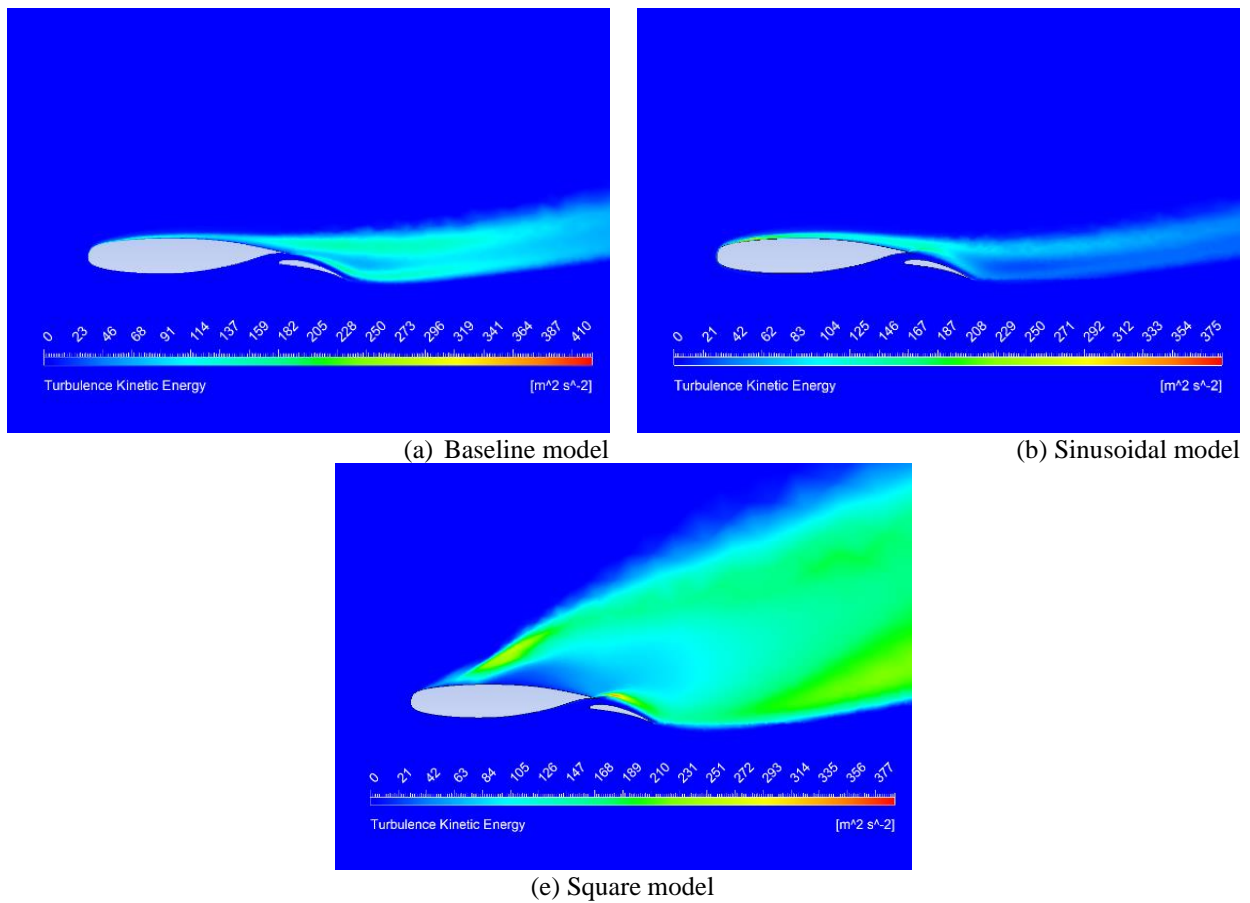


Fig. 15 Turbulent Kinetic Energy diagrams for $\lambda/h = 1.5$ models at $AOA = 17^\circ$, $Re=2.51E6$ and $Mach=0.185$

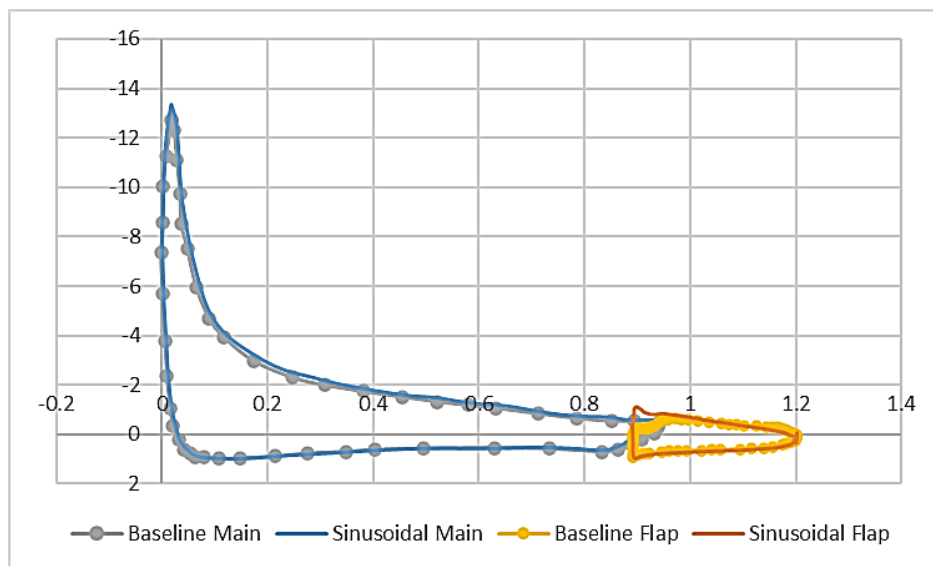


Fig. 16 C_p comparison of sinusoidal serration and baseline model at $AOA = 17^\circ$, $Re=2.51E6$, and $Mach=0.185$

conducted to compare the performance of three sinusoidal, square and triangular serrated models against a baseline model. Results indicated that serrations generate vortices that can significantly enhance the performance of the system at high incidence angles by delaying flow separation, increasing lift, and reducing drag. The sinusoidal model demonstrated the best performance, with a 19.5% increase in aerodynamic performance at a 17-degree angle of attack compared to the baseline model.

Additionally, it extended the stall angle by 2 degrees and increased the maximum lift coefficient by 6.8%. Vortex size and intensity directly influenced lift coefficient produced by the flap, and the square model with the largest vortices, experienced the highest increase in the lift coefficient generation of the flap (24.7%). The square model with a smaller wavelength-to-amplitude ($\lambda/h = 0.6$) ratio demonstrated average improvement of 1.2% in aerodynamic performance, and a 2.4 percent reduction in

drag coefficient compared to the model with ($\lambda/h = 1.5$) albeit with a lower maximum lift coefficient. Overall, serrations showed to have tremendous effect on the aerodynamic performance of the wing-flap assembly, especially at high incidence angles when high-lift devices are generally used. The current configuration showcases a potential for future industrial use in aviation and other industries that may require less complex passive control methods.

CONFLICT OF INTEREST

The authors have no conflicts to disclose.

AUTHORS CONTRIBUTION

S. Ahmadkhah: Writing – original draft, Visualization, Validation, Software & execution, Methodology, Investigation, Formal analysis, Data curation, Conceptualization; **A. Jahangirian:** Writing – review & editing, Supervision, Resources, Project administration, Methodology, Investigation, Conceptualization; **A. Zarinva:** Writing – original draft, Software & execution, Investigation, Conceptualization.

REFERENCES

- Alawadhi, H. A., Alex, A. G., & Kim, Y. H. (2014). *CFD analysis of wing trailing edge vortex generator using serrations*. EPJ Web of Conferences, 67, 02002. <https://doi.org/10.1051/epjconf/20146702002>
- Batchelor, G. K. (2000). *An introduction to fluid dynamics*. Cambridge University Press. <https://doi.org/10.1017/cbo9780511800955>
- Catalano, F., Lemes, R., & Brand, G. (Eds.). (2007). *Trailing edge treatment to enhance high lift system performance*. 1st CEAS European Air and Space Conference.
- Chandra, S., & Sharma, S. D. (2017). An experimental investigation to enhance the aerodynamic efficiency of micro aerial vehicle wing using bio-inspired serrations. *International Journal of Aeronautical and Space Sciences*, 22(5), 1042–1047. <https://doi.org/10.1007/s42405-021-00388-6>
- Ethiraj, L., & Pillai, S. N. (2021). Effect of trailing-edge modification over aerodynamic characteristics of NACA 0020 Airfoil. *Wind and Structures*, 33(6), 463–470. <https://doi.org/10.12989/was.2021.33.6.463>
- Gruber, M., Azarpeyvand, M., & Joseph, P. F. (2010). *Airfoil trailing edge noise reduction by the introduction of sawtooth and slitted trailing edge geometries* (pp. 1899–1907). International Congress on Acoustics. https://www.acoustics.asn.au/conference_proceeding/ICA2010/cdrom-ICA2010/papers/p686.pdf
- Hersh, A. S., & Hayden, R. E. (1971). *Aerodynamic sound radiation from lifting surfaces with and without leading-edge serrations*. NASA. <https://ntrs.nasa.gov/api/citations/19710026946/downloads/19710026946.pdf>
- Hussain, U., Malook, S. U., Shabir, B., Ali, O., & Ahmad, S. M. (2017). *Effect of trailing edge serration on the lift and drag characteristics of NACA0012 airfoil wing*. 35th AIAA Applied Aerodynamics Conference. <https://doi.org/10.2514/6.2017-4470>.
- Ichikawa, Y., Koike, S., Ito, Y., Murayama, M., Nakakita, K., Yamamoto, K., & Kusunose, K. (2021). Size effects of vane-type rectangular vortex generators installed on high-lift swept-back wing flap on lift force and flow fields. *Experiments in Fluids*, 62(8). <https://doi.org/10.1007/s00348-021-03198-4>.
- Jahangirian, A., & Johnston, L. (2007). *An efficient dual-time implicit method for high-lift aerodynamics using differential Reynolds-stress modelling*. 2nd European Conference for AeroSpace Sciences. https://usir.salford.ac.uk/2664/1/eucass_paper_2.13.01.pdf.
- Jawahar, H. K., Syamir A. S., Azarpeyvand, M., & Ilario, C. (2020). Aerodynamic and aeroacoustic performance of high-lift airfoil with serrated slat cusp. *AIAA AVIATION 2020 FORUM*. <https://doi.org/10.2514/6.2020-2554>.
- Ji, X., Wang, L., Ravi, S., Young, J., Lai, J. C. S., & Tian, F. (2023). Aerodynamic and aeroacoustic performance of a pitching foil with trailing edge serrations at a high Reynolds number. *Theoretical and Computational Fluid Dynamics*, 38(6), 825–844. <https://doi.org/10.1007/s00162-023-00677-8>.
- Khoshkhoo, R., & Jahangirian, A. (2016). Numerical simulation of flow separation control using multiple DBD plasma actuators. *Journal of Applied Fluid Mechanics*, 9(6), 1865–1875. <https://doi.org/10.18869/acadpub.jafm.68.235.25325>
- Knepper, A., & Garry, K. (2005). *A preliminary investigation of trailing edge serrations in high lift systems*. 35th AIAA Fluid Dynamics Conference and Exhibit. <https://doi.org/10.2514/6.2005-5261>.
- Liu, X., Ali, S. a. S., Azarpeyvand, M., & Mayer, Y. D. (2019). *Aeroacoustic and Aerodynamic study of trailing-edge serrated airfoils in tandem configuration* (pp. 5367–5374). 23rd International Congress on Acoustics. <https://research-information.bris.ac.uk/ws/files/239110159/000823.pdf>
- Naeni, H. K., Nili-Ahmadabadi, M., & Kim, K. C. (2019). An experimental study on the effect of a novel nature-inspired 3D-serrated leading edge on the aerodynamic performance of a double delta wing in the transitional flow regime. *Journal of Mechanical Science and Technology*, 33(12), 5913–5921. <https://doi.org/10.1007/s12206-019-1136-x>.
- Narsipur, S., Pomeroy, B., & Selig, M. (2012). *CFD analysis of multielement airfoils for wind turbines*.

- 30th AIAA Applied Aerodynamics Conference. <https://doi.org/10.2514/6.2012-2781>.
- Nemati, M., & Jahangirian, A. (2020). Robust aerodynamic morphing shape optimization for high-lift missions. *Aerospace Science and Technology*, 103, 105897. <https://doi.org/10.1016/j.ast.2020.105897>
- Saddoughi, S. G. (1994). *Experimental investigations of on-demand vortex generators* (pp. 197–203). NASA. <https://ntrs.nasa.gov/api/citations/19950016034/downloads/19950016034.pdf>
- Singh, S. K., Garg, M., Narayanan, S., Ayton, L., & Chaitanya, P. (2022). On the reductions of airfoil broadband noise through sinusoidal trailing-edge serrations. *Journal of Aerospace Engineering*, 35(2). [https://doi.org/10.1061/\(asce\)as.1943-5525.0001386](https://doi.org/10.1061/(asce)as.1943-5525.0001386)
- Tlua, B. A., & Joana, R. (2020). Optimization and testing of flat-plate trailing-edge serration geometry for reducing airfoil self-noise. *Canadian Acoustics*, 48(4), 7–18. <https://jcaa.caa-aca.ca/index.php/jcaa/article/view/3391>
- Van Den Berg, B., & Gooden, J. H. M. (1994). *Low-Speed surface pressure and boundary layer measurement data for the NLR 7301 Airfoil section with trailing edge flap*. AGARD AR 303 Vol-2. <https://www.sto.nato.int/publications/AGARD/AGARD-AR-303-VOL-2/AGARD-AR-303-Vol-2.pdf>
- Wei, Z., Wang, S., Farris, S., Chennuri, N., Wang, N., Shinsato, S., Demir, K., Horii, M., & Gu, G. X. (2024). Towards silent and efficient flight by combining bioinspired owl feather serrations with cicada wing geometry. *Nature Communications*, 15(1). <https://doi.org/10.1038/s41467-024-48454-3>
- Young, A. D. (1947). *The aerodynamic characteristics of flaps*. Aeronautical Research Council Reports and Memoranda. <https://apps.dtic.mil/sti/pdfs/ADA951553.pdf>